

Relative Dynamics and Control of Spacecraft Formations in Eccentric Orbits

Gökhan Inalhan*

Stanford University, Stanford, California 94305

and

Michael Tillerson[†] and Jonathan P. How[‡]

Massachusetts Institute of Technology, Cambridge, Massachusetts 02139

Formation flying is a key technology for both deep-space and orbital applications that involve multiple spacecraft. Many future space applications will benefit from using formation flying technologies to perform distributed observations (e.g., synthetic apertures for Earth mapping interferometry) and to provide improved coverage for communication and surveillance. Previous research has focused on designing passive apertures for these formation flying missions assuming a circular reference orbit. Those design approaches are extended and a complete initialization procedure for a large fleet of vehicles with an eccentric reference orbit is presented. The main result is derived from the homogenous solutions of the linearized relative equations of motion for the spacecraft. These solutions are used to find the necessary conditions on the initial states that produce T -periodic solutions that have the vehicles returning to the initial relative states at the end of each orbit, that is, $v(t_0) = v(t_0 + T)$. This periodicity condition and the resulting initialization procedure are originally given (in compact form) at the reference orbit perigee, but this is also generalized to enable initialization at any point around the reference orbit. In particular, an algorithm is given that minimizes the fuel cost associated with initializing the vehicle states (primarily the in-track and radial relative velocities) to values that are consistent with periodic relative motion. These algorithms extend and generalize previously published solutions for passive aperture forming with circular orbits. The periodicity condition and the homogenous solutions can also be used to estimate relative motion errors and the approximate fuel cost associated with neglecting the eccentricity in the reference orbit. The nonlinear simulations presented clearly show that ignoring the reference orbit eccentricity generates an error that is comparable to the disturbances caused by differential gravity accelerations.

Introduction

THE concept of autonomous formation flying of satellite clusters has been identified as an enabling technology for many future NASA and U.S. Air Force missions.^{1–4} Examples include the Earth Orbiter-1 mission that is currently on-orbit¹ (see also URL: <http://eo1.gsfc.nasa.gov/miscPages/home.html>), StarLight (URL: <http://starlight.jpl.nasa.gov/>), the Nanosat Constellation Trailblazer mission (URL: <http://nmp.jpl.nasa.gov/st5/>), and the Air Force TechSat-21 (URL: <http://www.vs.af.mil/factsheets/TechSat21.html>) distributed synthetic aperture radar (SAR). The use of fleets of smaller satellites instead of a single monolithic satellite should improve the science return through longer baseline observations, enable faster ground track repeats, and provide a high degree of redundancy and reconfigurability in the event of a single vehicle failure. If the ground operations can also be replaced with autonomous onboard control, this fleet approach should also decrease the mission cost at the same time.^{1,4} However, implementation of the distributed coordinating satellite concept will require tight maintenance and control of the relative distances and orientations between the participating satellites. Thus, the benefits of this approach come at a cost because the new systems architecture poses very stringent challenges in the areas of onboard sensing, high-level mission management and planning, and fleet-level fault detection/recovery.^{5,6}

The results in this paper focus on aspects of the mission planning in that they provide necessary conditions to initialize the vehicles on a passive aperture. By passive aperture, we mean a (short baseline) periodic formation configuration that provides good, distributed, Earth imaging, for example, with an SAR. These passive apertures have previously been designed using the closed-form solutions provided by Hill's equations (see Ref. 7) (also known as the Clohessy-Wiltshire equations), which are linearized about a circular reference orbit. There has also been analysis to develop apertures that are insensitive to differential J_2 disturbances based on nonlinear dynamic models (see Ref. 8).

This paper presents the complete initialization procedure for a large fleet of vehicles with an eccentric reference orbit. The work builds on earlier results by Lawden,⁹ Carter and Humi,¹⁰ and Carter¹¹ on the derivation and solution of the homogenous equations of relative motion for multiple spacecraft that are linearized about an eccentric reference orbit. (See Ref. 10 for an extensive historical perspective on the origin of these equations.) In particular, we provide the first presentation of the conditions necessary to initialize to a closed-form aperture on an eccentric orbit ($e \neq 0$). This is a key extension of the work by Carter/Lawden and an important point for future research on formation flying that previously had to use Hill's equations when working in a local vertical/local horizontal (LVLH) frame (see for example Refs. 12 and 13). This new initialization approach can also be used to estimate the fuel penalty associated with maintaining the fleet configuration with respect to an aperture designed using Hill's equation, even though the reference orbit is eccentric. This effect is shown to be significant, even for a typical shuttle orbit with $e = 0.005$.

The key periodicity result in this paper is derived in two ways. One way is based on the relative positions and velocities of the vehicles in an LVLH frame. Because this approach uses a set of linearized equations of relative motion, the periodicity condition is only as accurate as the linearization itself. However, numerous nonlinear simulations and analytic studies⁷ have shown that, for close formations, the linearized equations provide a very good representation

Received 26 June 2000; revision received 6 August 2001; accepted for publication 6 August 2001. Copyright © 2001 by the American Institute of Aeronautics and Astronautics, Inc. All rights reserved. Copies of this paper may be made for personal or internal use, on condition that the copier pay the \$10.00 per-copy fee to the Copyright Clearance Center, Inc., 222 Rosewood Drive, Danvers, MA 01923; include the code 0731-5090/02 \$10.00 in correspondence with the CCC.

*Research Assistant, Department of Aeronautics and Astronautics; ginalhan@stanford.edu. Student Member AIAA.

[†]Research Assistant, Department of Aeronautics and Astronautics; mike_t@mit.edu. Student Member AIAA.

[‡]Associate Professor, Department of Aeronautics and Astronautics; jhow@mit.edu. Senior Member AIAA.

of the relative motions of spacecraft about the appropriate reference orbit. We also derive the exact nonlinear condition from the differential energy matching condition using the orbital elements. With a consistent linearization approximation, it is then shown that an equivalent set of initialization conditions can be obtained in this second framework. Deriving the initialization condition from these two different perspectives provides additional insight on the periodicity constraint obtained using the linearized equations of relative motion.

The equations of motion used to derive the initialization to a passive aperture are valid for all reference orbit eccentricities, and so the results in this paper extend the recent work in Ref. 14. In particular, the initialization can be used in high-eccentricity types of orbits, such as Molniya, that enable missions with longer observation periods over particular regions of interest. For example, Figs. 1 and 2 show one such implementation for a reference orbit of $a = 46,000$ km, $e = 0.67$, and $i = 62.8$ deg. The in-plane and out-of-plane motion correspond to incremental changes in eccentricity ($\delta e = 0.0001$) and inclination ($\delta i = 0.005$). An interesting feature of these eccentric orbits is the figure-8-shaped out-of-plane motion. In comparison, small inclination differences for circular reference orbits only result in one-dimensional out-of-plane motion. This interesting feature of relative motion with eccentric orbits could be used to provide higher uv -plane coverage per orbit for aperture filling observations.

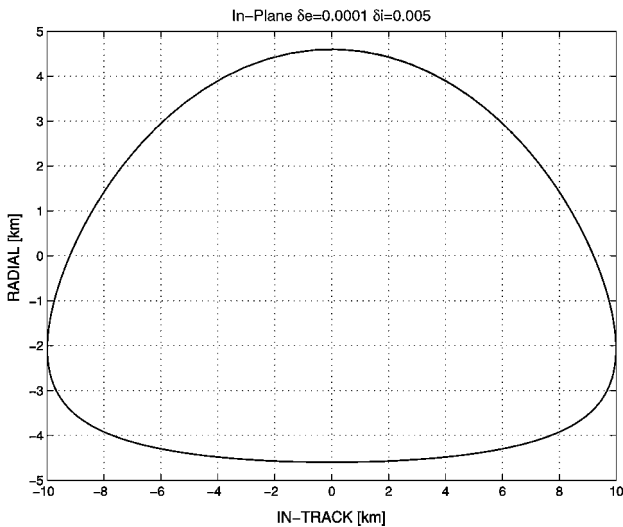


Fig. 1 In-plane formation for high-eccentricity reference orbit, nonlinear simulation for two orbits.

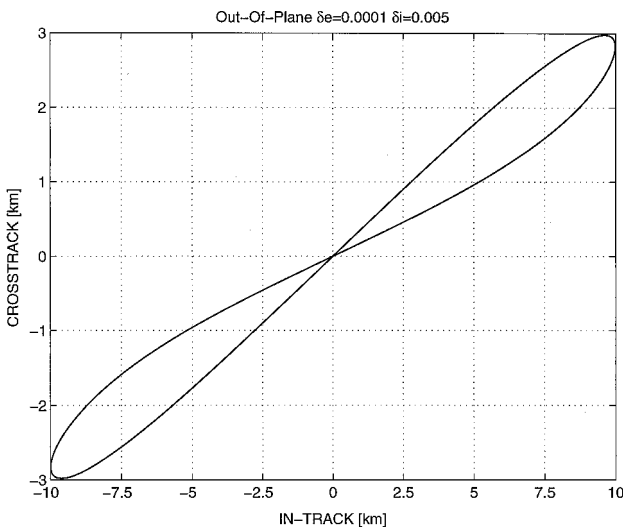


Fig. 2 Out-of-plane formation for high-eccentricity reference orbit, nonlinear simulation for two orbits.

The paper continues with a brief outline of the linearized equations of motion and their solution. These equations are used to form the monodromy matrix for the system, which is then used to solve for the periodicity condition. The next section generalizes the initialization process to other points on the reference orbit. The initialization is then analyzed using orbital elements. Finally, the homogeneous solutions are used to approximate the relative motion errors for in-plane and out-of-plane formations that neglect the reference orbit eccentricity during initialization. Also included is the effect of these errors on a standard feedback control scheme and the fuel cost associated with the necessary corrections.

Relative Dynamics in Eccentric Orbits

The following presents the dynamics for the relative motion of a satellite with respect to a reference satellite on an eccentric orbit. A brief development of the equations of motion appears hereafter, and the full details are available in Refs. 9–11 and 15. The location of each spacecraft within a formation is given by

$$\mathbf{R}_j = \mathbf{R}_{fc} + \boldsymbol{\rho}_j \quad (1)$$

where \mathbf{R}_{fc} and $\boldsymbol{\rho}_j$ correspond to the location of the formation center and the relative position of the j th spacecraft with respect to that point. The formation center can either be fixed to an orbiting satellite, or just a local point that provides a convenient reference for linearization. The reference orbit in the Earth-centered inertial (ECI) reference frame is represented by the standard orbital elements $(a, e, i, \Omega, \omega, \theta)$, which correspond to the semimajor axis, eccentricity, inclination, right ascension of the ascending node, argument of periaapsis, and true anomaly.

With the assumption that $|\boldsymbol{\rho}_j| \ll |\mathbf{R}_{fc}|$, the equations of motion of the j th spacecraft under the gravitational attraction of a main body

$${}_i\ddot{\mathbf{R}}_j = -(\mu/|\mathbf{R}_j|^3)\mathbf{R}_j + \mathbf{f}_j \quad (2)$$

can be linearized around the formation center to give

$${}_i\ddot{\boldsymbol{\rho}}_j = -\frac{\mu}{|\mathbf{R}_{fc}|^3}\left(\boldsymbol{\rho}_j - \frac{3\mathbf{R}_{fc} \cdot \boldsymbol{\rho}_j}{|\mathbf{R}_{fc}|^2}\mathbf{R}_{fc}\right) + \mathbf{f}_j \quad (3)$$

where the accelerations associated with other attraction fields, disturbances, or control inputs are included in \mathbf{f}_j . The derivatives in the ECI reference frame are identified by the preceding subscript i . A natural basis for inertial measurements and scientific observations is the orbiting (noninertial) reference frame Σ_c , fixed to the formation center (Fig. 3). By the use of kinematics, the relative acceleration observed in the inertial reference frame ${}_i\ddot{\boldsymbol{\rho}}_j$ can be related to the measurements in the orbiting reference frame

$${}_i\ddot{\boldsymbol{\rho}}_j = {}_c\ddot{\boldsymbol{\rho}}_j + 2{}_i\dot{\boldsymbol{\Theta}} \times {}_c\dot{\boldsymbol{\rho}}_j + {}_i\ddot{\boldsymbol{\Theta}} \times ({}_i\dot{\boldsymbol{\Theta}} \times \boldsymbol{\rho}_j) + ({}_i\ddot{\boldsymbol{\Theta}} \times \boldsymbol{\rho}_j) \quad (4)$$

where, ${}_i\dot{\boldsymbol{\Theta}}$ and ${}_i\ddot{\boldsymbol{\Theta}}$ correspond to the angular velocity and acceleration of this orbiting reference frame. The fundamental vectors $\boldsymbol{\rho}_j$, \mathbf{R}_{fc} , and ${}_i\dot{\boldsymbol{\Theta}}$ in Eqs. (3) and (4) can be expressed in Σ_c as

$$\boldsymbol{\rho}_j = x_j\hat{\mathbf{k}}_x + y_j\hat{\mathbf{k}}_y + z_j\hat{\mathbf{k}}_z \quad (5)$$

$$\mathbf{R}_{fc} = R_{fc}\hat{\mathbf{k}}_x \quad (6)$$

$${}_i\dot{\boldsymbol{\Theta}} = \dot{\theta}\hat{\mathbf{k}}_z \quad (7)$$

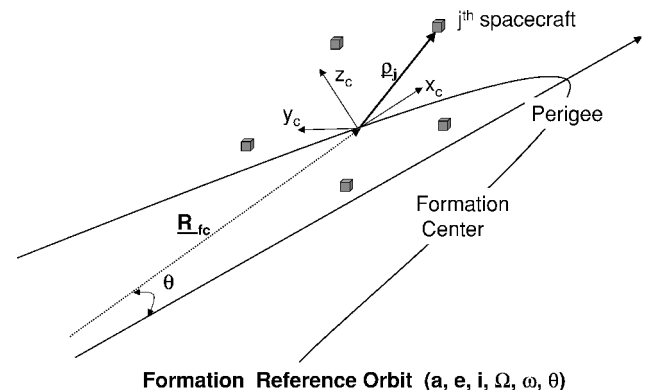


Fig. 3 Relative motion in formation reference frame.

where the unit vector \hat{k}_x points radially outward from Earth's center (antinadir pointing) and \hat{k}_y is in the in-track direction along increasing true anomaly. This right-handed reference frame is completed with \hat{k}_z , pointing in the cross-track direction. All of the proceeding vectors and their time rate of changes are expressed in the orbiting reference frame Σ_c .

When Eqs. (3) and (4) are combined to obtain an expression for ${}^c\dot{\rho}_j$, and Eqs. (5-7) are used, it is clear that the linearized relative dynamics with respect to an eccentric orbit can be expressed via a unique set of elements and their time rate of change. This set consists of the relative states $[x_j, y_j, z_j]$ of each satellite, the radius R_{fc} , and the angular velocity $\dot{\theta}$ of the formation center. Using fundamental orbital mechanics describing planetary motion,^{16,17} the radius and angular velocity of the formation center can be written as

$$|R_{fc}| = \frac{a(1-e^2)}{1+e\cos\theta}, \quad \dot{\theta} = \frac{n(1+e\cos\theta)^2}{(1-e^2)^{3/2}} \quad (8)$$

where $n = (\mu/a^3)^{1/2}$ is the natural frequency of the reference orbit. These expressions can be substituted into the equation for ${}^c\dot{\rho}_j$ to obtain the relative motion of the j th satellite in the orbiting formation reference frame

$$\begin{aligned} \frac{d}{dt} \begin{bmatrix} \dot{x} \\ \dot{y} \\ \dot{z} \end{bmatrix}_j &= -2 \begin{bmatrix} 0 & -\dot{\theta} & 0 \\ \dot{\theta} & 0 & 0 \\ 0 & 0 & 0 \end{bmatrix} \begin{bmatrix} \dot{x} \\ \dot{y} \\ \dot{z} \end{bmatrix}_j - \begin{bmatrix} -\dot{\theta}^2 & 0 & 0 \\ 0 & -\dot{\theta}^2 & 0 \\ 0 & 0 & 0 \end{bmatrix} \\ &\times \begin{bmatrix} x \\ y \\ z \end{bmatrix}_j - \begin{bmatrix} 0 & -\ddot{\theta} & 0 \\ \ddot{\theta} & 0 & 0 \\ 0 & 0 & 0 \end{bmatrix} \begin{bmatrix} x \\ y \\ z \end{bmatrix}_j + n^2 \left(\frac{1+e\cos\theta}{1-e^2} \right)^3 \\ &\times \begin{bmatrix} 2x \\ -y \\ -z \end{bmatrix}_j + \begin{bmatrix} f_x \\ f_y \\ f_z \end{bmatrix}_j \end{aligned} \quad (9)$$

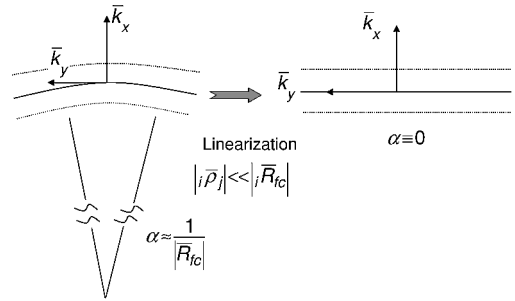


Fig. 4 Mapping from curvilinear to linear space.

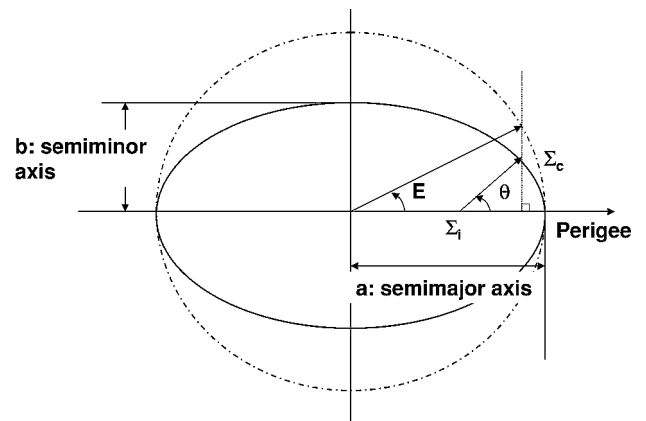


Fig. 5 Orbital plane, true and eccentric anomaly.

With these transformations, the set of linear time-varying (LTV) equations describing the relative motion of the j th spacecraft in an eccentric orbit can be written as

$$\frac{d}{d\theta} \begin{bmatrix} x' \\ x \\ y' \\ y \end{bmatrix}_j = \begin{bmatrix} \frac{2e\sin\theta}{1+e\cos\theta} & \frac{3+e\cos\theta}{1+e\cos\theta} & 2 \\ 1 & 0 & 0 \\ -2 & \frac{2e\sin\theta}{1+e\cos\theta} & \frac{2e\sin\theta}{1+e\cos\theta} \\ 0 & 0 & 1 \end{bmatrix} \begin{bmatrix} x' \\ x \\ y' \\ y \end{bmatrix}_j + \frac{(1-e^2)^3}{(1+e\cos\theta)^4 n^2} \begin{bmatrix} 1 & 0 \\ 0 & 0 \\ 0 & 1 \\ 0 & 0 \end{bmatrix} \begin{bmatrix} f_x \\ f_y \end{bmatrix}_j \quad (11)$$

The terms on the right-hand side of this equation correspond to the Coriolis acceleration, centripetal acceleration, accelerating rotation of the reference frame, and the virtual gravity gradient terms with respect to the formation reference. The right-hand side also includes the combination of other external disturbances and control accelerations in f_j .

Note that care must be taken when interpreting and using the equations of motion and the relative states in a nonlinear analysis. The difficulty results from the linearization process, which maps the curvilinear space to a rectangular one by a small curvature approximation. Figure 4 shows the effects of the linearization and the small curvature assumption. In this case, a relative separation in the in-track direction in the linearized equations actually corresponds to an incremental phase difference in true anomaly θ .

Although Eq. (9) is expressed in the time domain, monotonically increasing true anomaly θ of the reference orbit provides a natural basis for parameterizing the fleet time and motion.¹⁰ This observation is based on the fact that the angular velocity and the radius describing the orbital motion are functions of the true anomaly, as shown in Fig. 5. When θ is used as the free variable, the equations of motion can be transformed using the relationships

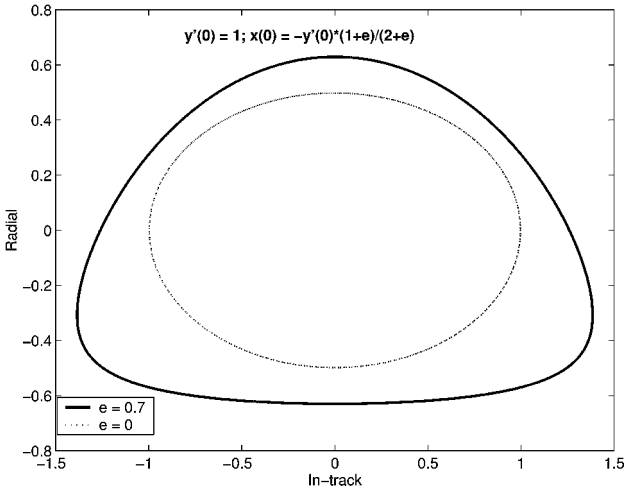
$$(\dot{\cdot}) = (\cdot)' \dot{\theta}, \quad (\ddot{\cdot}) = (\cdot)'' \dot{\theta}^2 + \dot{\theta} \dot{\theta}' (\cdot)' \quad (10)$$

$$\begin{aligned} \frac{d}{d\theta} \begin{bmatrix} z' \\ z \end{bmatrix}_j &= \begin{bmatrix} \frac{2e\sin\theta}{1+e\cos\theta} & \frac{-1}{1+e\cos\theta} \\ 1 & 0 \end{bmatrix} \begin{bmatrix} z' \\ z \end{bmatrix}_j \\ &+ \frac{(1-e^2)^3}{(1+e\cos\theta)^4 n^2} \begin{bmatrix} 1 \\ 0 \end{bmatrix} f_{zj} \end{aligned} \quad (12)$$

As shown, the in-plane (x and y) and out-of-plane (z) motions are decoupled and can be expressed separately. Equation (11) gives the in-plane relative motion of the spacecraft with respect to the formation center in the true anomaly domain. The out-of-plane relative dynamics in Eq. (12) correspond to the typical cyclic behavior that is observed as a result of small changes in the inclination and/or right ascension of the ascending node of the spacecraft with respect to the formation reference frame.

As given in Refs. 9, 11, and 15 the homogenous solutions to these LTV differential equations of motion are

$$x(\theta)_j = \sin\theta [d_{1j}e + 2d_{2j}e^2 H(\theta)] - \cos\theta \left[\frac{d_{2j}e}{(1+e\cos\theta)^2} + d_{3j} \right] \quad (13)$$


 Fig. 6 Closed-form in-plane motion for $e = 0.7$.

$$y(\theta)_j = \left[d_{1j} + \frac{d_{4j}}{(1 + e \cos \theta)} + 2d_{2j}eH(\theta) \right] + \sin \theta \left[\frac{d_{3j}}{(1 + e \cos \theta)} + d_{3j} \right] + \cos \theta \left[d_{1j}e + 2d_{2j}e^2H(\theta) \right] \quad (14)$$

$$z(\theta)_j = \sin \theta \left[\frac{d_{5j}}{(1 + e \cos \theta)} \right] + \cos \theta \left[\frac{d_{6j}}{(1 + e \cos \theta)} \right] \quad (15)$$

The d_{ij} in these solutions are integration constants for each spacecraft, and they are calculated from the corresponding initial conditions. Two further important relationships are

$$H(\theta) = \int_{\theta_0}^{\theta} \frac{\cos \theta}{(1 + e \cos \theta)^3} d\theta = -(1 - e^2)^{-\frac{3}{2}} \times \left[\frac{3eE}{2} - (1 + e^2) \sin E + \frac{e}{2} \sin E \cos E + d_H \right] \quad (16)$$

$$\cos E = \frac{e + \cos \theta}{1 + e \cos \theta} \quad (17)$$

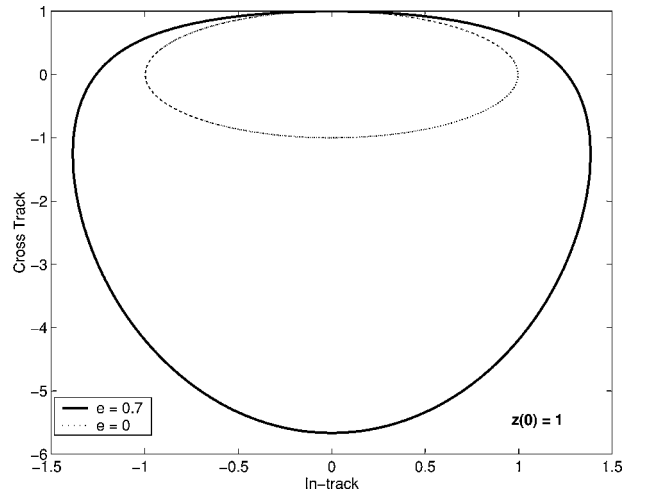
where E is the eccentric anomaly that can be expressed as a function of the true anomaly. Also, d_H is the integration constant calculated from $H(\theta_0) = 0$. For a typical case where $\theta_0 = 0$, d_H is also zero.

Remark 1: These solutions are available in the literature in various forms using different reference frames and variables. The first derivation with singularities in the closed-form solution was provided by Lawden in 1963.⁹ The results by Carter,¹¹ with the singularities removed from the solutions, forms the basis of our analysis. These homogenous solutions are extremely useful for well-behaved numerical and analytical analysis on the shape, structure, and optimization of passive apertures in eccentric reference orbits. Also note that the same solutions can be obtained via incremental changes in orbital elements, as presented by Marec.¹⁵ \square

Figures 6 and 7 show an example of the relative motion of two spacecraft when the reference orbit eccentricity is $e = 0.7$. In this particular case, the spacecraft in the formation are initialized to provide a periodic uv -plane (observing plane) coverage. The changes in the closed-form solution from the typical Hill's equation result ($e = 0$) are readily apparent in the figures. The next section presents the necessary conditions for initializing to these periodic solutions.

Monodromy Matrix and Periodicity Conditions

The ability to form exact passive apertures requires the existence of periodic solutions to the unforced equations of motion.⁷ As indicated by Eq. (15), the out-of-plane dynamics are naturally periodic as a result of the geometry of the problem. For the in-plane motion, Eqs. (13) and (14) represent the unforced closed-form solutions. Note that both the in-track (y) and radial (x) components consist of


 Fig. 7 Closed-form out-of-plane motion for $e = 0.7$.

either constants, sinusoidal terms, or terms that include $H(\theta)$, which are the only ones that show diverging behavior. For both of these equations, the coefficient d_{2j} , which is a function of initial relative states, multiplies $H(\theta)$. Thus, any periodic solution will require that this coefficient be zero. It can be demonstrated that the linear time-varying equations describing the in-plane motion in Eq. (11) have a nontrivial periodic solution using the following result.

Theorem: Given an LTV dynamic description of

$$\dot{v}(t) = A(t)v(t), \quad v(t_0) = v_0 \quad (18)$$

$$v(t) = \Phi(t, \tau)v(\tau) \quad (19)$$

where $A(t)$ is T periodic, that is, $A(t + T) = A(t)$. For any t_0 , there exists a nonzero initial state v_0 such that the solution $v(t)$ is T periodic [i.e., $v(t_0) \neq 0$ and $v(t_0 + T) = v(t_0)$] if and only if at least one eigenvalue of $\Phi(T, 0)$ is unity.

Proof: See Ref. 18.

Here $[\Phi(t, \tau) : v(\tau) \rightarrow v(t)]$ is the fundamental matrix that describes the mapping of a particular initial condition $v(\tau)$ through the dynamics. For the case $t - \tau = T$, the fundamental matrix takes a special form called a monodromy matrix,¹⁹ which can be used to analyze both the orbit periodicity and stability. If there exists a T -periodic mapping (where T is the orbit period), the base configuration is a fixed point.

Note that the A matrix of the in-plane dynamics in Eq. (11) is T periodic because all elements are either constant or sinusoidal in θ . Thus, to demonstrate that the relative orbital motion is periodic, we must find the transformation matrix that maps the initial states at ($\theta_0 = 0$) to the final states at ($\theta_f = 2\pi$) and then prove that $\Phi(2\pi, 0)$ has at least one eigenvalue equal to one. (It is assumed in this section that the initialization is done at $\theta_0 = 0$, but this is generalized in the following subsections to other values of $\theta \neq 0$.) After some manipulation (see Appendix A for the full details), for the initial conditions at $\theta_0 = 0$, the integration constants from Eqs. (13) and (14) can be expressed as a function of the initial states v_0

$$\begin{bmatrix} d_1 \\ d_2 \\ d_3 \\ d_4 \end{bmatrix}_j = \begin{bmatrix} p_{11} & 0 & 0 & 0 \\ 0 & p_{22} & p_{23} & 0 \\ 0 & p_{32} & p_{33} & 0 \\ p_{41} & 0 & 0 & p_{44} \end{bmatrix} \begin{bmatrix} x'(0) \\ x(0) \\ y'(0) \\ y(0) \end{bmatrix}_j \quad (20)$$

with corresponding values of the matrix elements

$$\begin{aligned} p_{11} &= 1/e, & p_{22} &= (2 + e)(1 + e)^2/e^2, & p_{23} &= (1 + e)^3/e^2 \\ p_{32} &= -[2(1 + e)/e], & p_{33} &= -[(1 + e)/e] \\ p_{41} &= -[(1 + e)^2/e], & p_{44} &= (1 + e) \end{aligned} \quad (21)$$

The final states (at $\theta_f = 2\pi$) can also be written in terms of the integration constants

$$\begin{bmatrix} x'(2\pi) \\ x(2\pi) \\ y'(2\pi) \\ y(2\pi) \end{bmatrix}_j = \begin{bmatrix} w_{11} & w_{12} & 0 & 0 \\ 0 & w_{22} & w_{23} & 0 \\ 0 & w_{32} & w_{33} & 0 \\ w_{41} & w_{42} & 0 & w_{44} \end{bmatrix} \begin{bmatrix} d_1 \\ d_2 \\ d_3 \\ d_4 \end{bmatrix}_j \quad (22)$$

with the corresponding values of the matrix elements

$$w_{11} = e, \quad w_{12} = 2e^2 H(2\pi), \quad w_{22} = -[e/(1+e)^2]$$

$$w_{23} = -1, \quad w_{32} = 2eH'(2\pi)(1+e)$$

$$w_{33} = (2+e)/(1+e), \quad w_{41} = 1+e$$

$$w_{42} = 2eH(2\pi)(1+e), \quad w_{44} = 1/(1+e)$$

$$H(2\pi) = -[3\pi e / (1 - e^2)^{\frac{5}{2}}], \quad H'(2\pi) = 1/(1+e)^3 \quad (23)$$

The integration constants expressed as a function of the initial states from Eq. (20) can be combined with Eq. (22) to describe the final states. Then, by the use of the matrix elements described by Eqs. (21) and (23), Eq. (22) can be rewritten as (full details in Appendix A)

$$\begin{bmatrix} x'(2\pi) \\ x(2\pi) \\ y'(2\pi) \\ y(2\pi) \end{bmatrix}_j = \begin{bmatrix} 1 & w_{12}p_{22} & w_{12}p_{23} & 0 \\ 0 & 1 & 0 & 0 \\ 0 & 0 & 1 & 0 \\ 0 & w_{42}p_{22} & w_{42}p_{23} & 1 \end{bmatrix} \begin{bmatrix} x'(0) \\ x(0) \\ y'(0) \\ y(0) \end{bmatrix}_j \quad (24)$$

$$\Rightarrow v_j(2\pi) = \Phi_j(2\pi, 0)v_j(0) \quad (25)$$

The transformation matrix in Eq. (25) is the fundamental matrix of the LTV system at $\theta_f = 2\pi$ scaled by its value at $\theta_0 = 0$. Because all eigenvalues of the transformation matrix in Eq. (25) are equal to 1, the result given can be used to obtain T -periodic solutions for this system when $0 < e < 1$.

The following sections continue with the analysis of the transformation matrix to obtain conditions on the vehicle states that yield nontrivial periodic motions. Note that these periodicity conditions are only as accurate as the linearized relative motion model used in their derivation. However, numerous nonlinear simulations and analytic studies⁷ have shown that, for close formations, the linearized equations provide a very good representation of the relative motions of spacecraft about the appropriate reference orbit.

Initialization

As given earlier, a solution is T periodic if $v_j(2\pi) = v_j(0)$. This is clearly true for y' , the in-track velocity differences, and x , the relative radial position. However, to ensure that

$$y(2\pi) = y(0), \quad x'(2\pi) = x'(0) \quad (26)$$

it follows directly from Eq. (24) that

$$w_{12}[p_{22}x(0) + p_{23}y'(0)] \equiv 0 \quad (27)$$

$$w_{42}[p_{22}x(0) + p_{23}y'(0)] \equiv 0 \quad (28)$$

With $e \neq 0$, both w_{12} and w_{42} are nonzero, and so these constraints both require that $p_{22}x(0) + p_{23}y'(0) \equiv 0$, which gives the periodicity or no-drift condition at $\theta_0 = 0$

$$y'(0)/x(0) = -(p_{22}/p_{23}) = -[(2+e)/(1+e)] \quad (29)$$

This condition provides a relationship between the initial radial position $x(0)$ and in-track velocity differences $y'(0)$ that must be used to obtain a periodic relative motion of the spacecraft. Here $y'(0)$ corresponds to the true anomaly rate of change of the in-track relative position, as observed in the noninertial formation reference frame. Note that the periodicity condition does not constrain $y(0)$ (corresponds to phasing in the true anomaly of the spacecraft) and $x'(0)$

(corresponds to an incremental radial velocity difference as a result of radial firing at $\theta = 0$). As defined earlier, $\theta = 0$ corresponds to the formation center being at the perigee of the reference orbit, which does not necessarily correspond to each spacecraft in the formation being at their individual orbit perigees. These extra degrees of freedom coming from radial relative velocity (in transformed form) $x'(0)$ and in-track separation $y(0)$ can be used to define the shape and scale of the relative motion, and they are consistent with the extra degrees of freedom that exist in the related no-drift solutions associated with Hill's equations.

In applications that do not require absolute orbital element matching, the only condition for passive apertures is that the drift rates be matched, that is, $[y'(0)/x(0)]_j$ is the same for all spacecraft. This is identical to redefining the formation center to a reference orbit that matches the natural frequency of the aperture vehicles and, thus, obtaining no-drift conditions with respect to this new formation center. Such an approach is shown in the results of Fig. 1.

Equation (29) can also be expressed in the time domain as

$$\frac{\dot{y}(0)}{x(0)} = -\frac{n(2+e)}{(1+e)^{\frac{1}{2}}(1-e)^{\frac{3}{2}}} \quad (30)$$

Note that, as $e \rightarrow 0$, Eq. (30) converges to the differential energy equalization condition for a circular reference orbit, that is, $\dot{y}(0)/x(0) = -2n$. This condition can easily be identified from the homogenous solution of the Cholesy-Wiltshire equations describing the linearized relative dynamics with respect to a circular reference orbit (see Ref. 17).

Also note that a set of initialization conditions can be derived using the orbital elements and their incremental changes, as is shown later in this paper. That approach demonstrates that the periodicity or no-drift condition is equivalent to the linearized form of the zero-differential energy condition. The following generalizes the initialization procedure to other values of θ .

General Initialization

The initialization for periodic motion at other values of θ can also be obtained using Eqs. (13), (14), (A1), and (A2). For example, consider a spacecraft at some $\theta_d \neq 0$ with current values of the scaled position and velocities given by $x(\theta_d)$, $y(\theta_d)$, $x'(\theta_d)$, and $y'(\theta_d)$. When it is assumed that these values are not consistent with a periodic solution, they can be modified using Eq. (29). To start, first use Eqs. (13), (14), (A1), and (A2) to define

$$\begin{bmatrix} x(\theta_d) \\ y(\theta_d) \\ x'(\theta_d) \\ y'(\theta_d) \end{bmatrix} = \begin{bmatrix} r_1 \\ r_2 \\ r_3 \\ r_4 \end{bmatrix} \begin{bmatrix} d_1 \\ d_2 \\ d_3 \\ d_4 \end{bmatrix} \equiv RD \quad (31)$$

$$\begin{bmatrix} x(0) \\ y'(0) \end{bmatrix} = \begin{bmatrix} r_{30} \\ r_{40} \end{bmatrix} D \quad (32)$$

where the r_i are the appropriate row vectors of coefficients for the d_i and r_{i0} is the row vector of coefficients evaluated at $\theta = 0$. Equation (29) constrains the relationship between $y'(0)$ and $x(0)$, which can be rewritten using Eq. (32) as

$$\{-(2+e)/(1+e)\}r_{30} - r_{40}D = 0 \quad (33)$$

Note that it is straightforward to demonstrate from this expression that the periodicity constraint is equivalent to setting $d_2 = 0$. To complete the initialization process, we assume that $x(\theta_d)$ and $y(\theta_d)$ are constrained to the values provided earlier and that only the values of $y'(\theta_d)$ and $x'(\theta_d)$ can be changed to achieve periodic motion. These assumptions provide a total of three constraints on the four unknowns (the d_i). The fourth constraint can be developed in a variety of ways, depending on the mission objectives, and several alternatives are detailed in the following.

Symmetric Motion

For example, one approach would be to constrain the periodic motion so that it is symmetric in-track about the origin. Using $y(\theta)$

from Eq. (14) evaluated at $\theta = 0$ and π and setting the average to zero yields the constraint

$$[1 \quad e(1+e)H(0) + e(1-e)H(\pi) \quad 0 \quad (1-e^2)^{-1}]D = 0 \quad (34)$$

Appending this constraint to the three given earlier would completely define one type of periodic motion.

Fuel Optimized

In general, the symmetric initialization requires that both $x'(\theta_d)$ and $y'(\theta_d)$ be modified, which can be fuel intensive. This naturally leads to the question of whether there is a way to select the d_i that minimizes the fuel cost associated with changing $x'(\theta_d)$ and/or $y'(\theta_d)$. One solution to this problem is to pose it as an optimization that minimizes the ΔV required to obtain the initial velocities that would be consistent with periodic relative motion starting at θ_d . To proceed, define the desired velocities for periodic motion $x'(\theta_d)_{\text{des}}$ and $y'(\theta_d)_{\text{des}}$ in terms of the given initial velocities, $x'(\theta_d)_{\text{init}}$ and $y'(\theta_d)_{\text{init}}$, and the required incremental velocity changes, ΔV_x and ΔV_y , as

$$x'(\theta_d)_{\text{des}} = x'(\theta_d)_{\text{init}} + \Delta V_x, \quad y'(\theta_d)_{\text{des}} = y'(\theta_d)_{\text{init}} + \Delta V_y \quad (35)$$

The $x'(\theta_d)_{\text{des}}$ and $y'(\theta_d)_{\text{des}}$ can be written in terms of the d_i using Eq. (31), and so the total ΔV can be expressed in terms of the given initial values and the unknown d_i . When the slack variables ΔV^+ and ΔV^- are introduced for each ΔV , the optimization problem can be written as the linear program (LP):

$$\begin{aligned} J &= \min c^T U \\ \text{subject to } & A_{\text{eq}} U = b_{\text{eq}} \\ & A_{\text{ineq}} U \leq b_{\text{ineq}} \end{aligned} \quad (36)$$

where

$$U^T = [\Delta V_x^+ \quad \Delta V_x^- \quad \Delta V_y^+ \quad \Delta V_y^- \quad d_1 \quad d_2 \quad d_3 \quad d_4] \quad (37)$$

$$c^T = [1 \quad 1 \quad 1 \quad 1 \quad 0 \quad 0 \quad 0 \quad 0] \quad (38)$$

$$A_{\text{eq}} = \begin{bmatrix} 1 & -1 & 0 & 0 & & & & -r_3 \\ 0 & 0 & 1 & -1 & & & & -r_4 \\ 0 & 0 & 0 & 0 & & & & r_1 \\ 0 & 0 & 0 & 0 & & & & r_2 \\ 0 & 0 & 0 & 0 & & & & -[(2+e)/(1+e)]r_{30} - r_{40} \end{bmatrix} \quad (39)$$

$$b_{\text{eq}} = \begin{bmatrix} -x'(\theta_d)_{\text{init}} \\ -y'(\theta_d)_{\text{init}} \\ x(\theta_d) \\ y(\theta_d) \\ 0 \end{bmatrix} \quad (40)$$

and A_{ineq} is an 4×8 matrix of zeros with $(A_{\text{ineq}})_{11} = (A_{\text{ineq}})_{22} = (A_{\text{ineq}})_{33} = (A_{\text{ineq}})_{44} = -1$ and b_{ineq} is an 4×1 vector of zeros. These inequality constraints force the slack variables to be positive. The LP problem has four variables and nine constraints. The equality constraint satisfies the position constraints in Eq. (31), the velocity constraints in Eq. (35), and the periodicity constraint in Eq. (33). The solution of the LP problem contains the four d_i and the ΔV required to change the given initial velocities to the desired velocities for periodic motion.

The LP problem was tested on a variety of different cases, and the solution always resulted in only a change in the in-track velocity to meet the periodicity constraint. The radial velocity remained unchanged from the (potentially random) initial value that was provided to the problem. This suggests the following simple alternative solution.

Velocity Constraint

The final formulation simply imposes the constraint that the radial velocity not change from the initial value provided. Thus, $x(\theta_d)$, $y(\theta_d)$, and $x'(\theta_d)$ must be the values provided earlier, and only $y'(\theta_d)$ can be changed by the initialization process. The periodicity constraint in Eq. (33) then provides the fourth constraint:

$$\begin{bmatrix} x(\theta_d) \\ y(\theta_d) \\ x'(\theta_d) \\ 0 \end{bmatrix} = \begin{bmatrix} r_1 \\ r_2 \\ r_3 \\ \{-(2+e)/(1+e)\}r_{30} - r_{40} \end{bmatrix} D \equiv \tilde{R}D$$

In this case the constants of integration in the problem are given by

$$D = \tilde{R}^{-1} \begin{bmatrix} x(\theta_d) \\ y(\theta_d) \\ x'(\theta_d) \\ 0 \end{bmatrix}$$

which then completely defines the initialization process for any value of θ .

Examples

Sample initializations and the resulting trajectories are presented in Figs. 8 and 9. The initializations were determined for $\theta_d = 5$ and

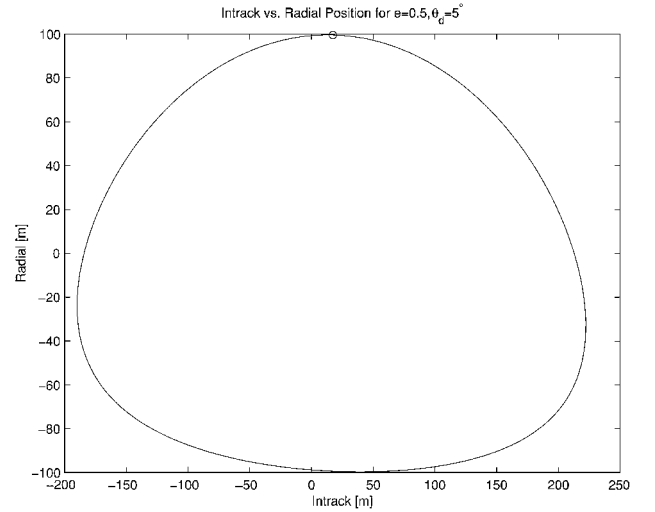


Fig. 8 Initialization ($\theta_d = 5$ deg) and trajectory for four orbits, \circ represents initial constrained position.

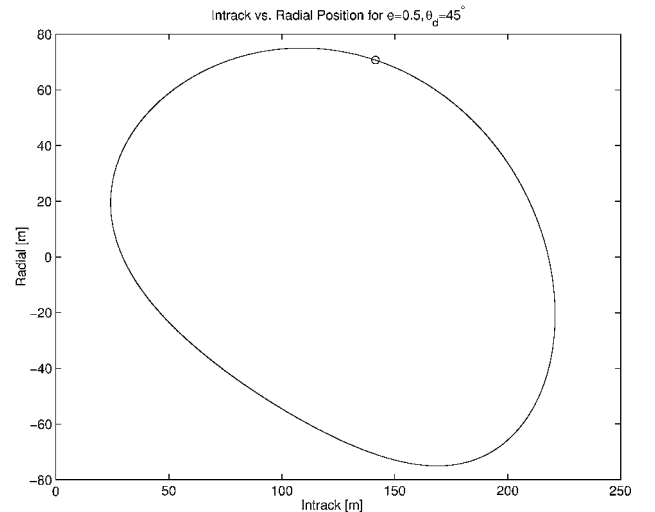


Fig. 9 Initialization ($\theta_d = 45$ deg) and trajectory for four orbits, \circ represents initial constrained position.

45 deg and simulated in a commercially available high-fidelity non-linear orbit propagator. The \circ represents the given initial position. The trajectory was propagated for four orbits using the initial conditions determined by the LP initialization approach. As shown, there is no noticeable drift in either example. The results with $\theta_d = 5$ deg are similar to those shown in Fig. 1, which were initialized at $\theta_d = 0$ deg using Eq. (30). However, the resulting periodic motions at larger values of θ are quite complicated, and, as is clearly shown for the case initialized at $\theta_d = 45$ deg, the periodic motion is not necessarily centered about the origin.

Periodicity Conditions: Orbital Approach

This section presents the necessary conditions for obtaining a no-drift solution in eccentric orbits using the orbital elements. The energy level of the reference orbit¹⁶ with orbital frequency $n = (\mu/a^3)^{1/2}$ and gravitational constant μ is given by

$$\varepsilon = -(\mu/2a) = -[(n\mu)^{2/3}/2] \quad (41)$$

The necessary condition to obtain the no-drift conditions is that $\varepsilon = \varepsilon_i \forall i \in \{1, 2, \dots, N\}$, which effectively matches the orbital periods of the N satellites to the formation center. At the perigee for the formation center, the energy difference between the i th satellite and the formation center can be written as

$$\delta\varepsilon_i = \varepsilon_i - \varepsilon = (V_{p_i}^2/2 - \mu/r_{p_i}) - (V_p^2/2 - \mu/r_p) \quad (42)$$

Thus, the condition for zero differential energy is that

$$V_{p_i}^2 - V_p^2 = 2\mu \left(\frac{r_p - r_{p_i}}{r_p r_{p_i}} \right) \quad (43)$$

By the use of the following relation for eccentricity

$$e = (r_a - r_p)/(r_a + r_p) = 1 - r_p/a \quad (44)$$

(r_a and r_p correspond to the orbital radius at apogee and perigee), the eccentricity difference can be written as an incremental change in perigee radius δr_i

$$\begin{aligned} \delta e_i &= e_i - e = (1 - r_{p_i}/a) - (1 - r_p/a) \\ &= -[(r_{p_i} - r_p)/a] = -(\delta r_i/a) \end{aligned} \quad (45)$$

By the use of Eqs. (44) and (45), Eq. (43) can be rewritten as

$$\begin{aligned} \frac{V_{p_i}}{V_p} &= \sqrt{1 - \frac{2\mu}{V_p^2} \left[\frac{\delta r_i}{a^2(1-e)(1-e_i)} \right]} \\ &= \sqrt{1 + \frac{2\mu}{aV_p^2} \left[\frac{\delta e_i}{(1-e)(1-e_i)} \right]} \end{aligned} \quad (46)$$

which is the exact expression for differential energy matching. Note that satisfying this condition is complicated by the coupling that exists between V_{p_i} and e_i [shown in Eq. (48)]. This final expression can be approximated as

$$V_{p_i}/V_p \cong 1 + (\mu/aV_p^2) [\delta e_i/(1-e)^2] \quad (47)$$

assuming that $|\delta e_i| \ll 1$ and using $V_p \geq V_{cs}$. Here $V_{cs} = (\mu/a)^{1/2}$ is the circular velocity for a given semimajor axis a . The statement that $V_p \geq V_{cs}$ comes directly from the fact that the perigee velocity can be defined¹⁶ as

$$V_p^2 = \frac{\mu(1-e^2)}{a(1-e)^2} = \frac{\mu(1+e)}{a(1-e)} \quad (48)$$

so that $V_p \geq V_{cs}$ for any $0 \leq e < 1$.

When an eccentric reference orbit ($0 < e < 1$) is focused on, with $|\delta e_i| \ll e$, Eq. (47) becomes

$$\delta V_{p_i} \cong (\mu/aV_p) [\delta e_i/(1-e)^2] = -(\mu/a^2V_p) [\delta r_i/(1-e)^2] \quad (49)$$

where the eccentricity difference has been replaced with a perigee radius difference. Then, by the use of Eq. (48), Eq. (49) can be reformulated as

$$\delta V_{p_i} \cong -\frac{\mu}{a^2} \frac{a^{1/2}(1-e)}{\mu^{1/2}(1-e)^{3/2}} \frac{\delta r_i}{(1-e)^2} = -\frac{\mu^{1/2}}{a^{3/2}} \frac{\delta r_i}{(1-e)^{3/2}(1+e)^{1/2}} \quad (50)$$

to obtain

$$\delta V_{p_{iabs}} = \delta V_{p_i} \cong -\frac{n\delta r_i}{(1-e)^{3/2}(1+e)^{1/2}} \quad (51)$$

Essentially, this necessary condition for differential energy matching accounts for the difference in perigee radius. Note that δr_i actually represents an eccentricity difference, as described in Eq. (45).

By the use of the kinematic relationship $\delta \mathbf{V}_{abs} = \delta \mathbf{V}_{rel} + \boldsymbol{\omega} \times \delta \mathbf{r}$, the differential velocity in the linearized framework, that is, Fig. 4, with respect to a reference attached to the formation center can be calculated for a given geometry. As discussed earlier, the linearization maps the curvilinear space to a rectangular one. As such, with the geometry shown in Fig. 4 at $\theta = 0$, $\delta V_{p_{i,rel}}$ and δr_i correspond to the relative in-track velocity y' and radial separation x , respectively. Using this fact and $\omega = \dot{\theta}(0)$, where

$$\dot{\theta}(0) = \frac{n(1+e)^2}{(1-e^2)^{3/2}} = \frac{n(1+e)}{(1-e)^{3/2}(1+e)^{1/2}}$$

the relative velocity increment as observed by the formation center can be written as

$$\delta V_{p_{i,rel}} \cong -\frac{n(2+e)\delta r_i}{(1-e)^{3/2}(1+e)^{1/2}} \quad (52)$$

Equation (52) is the same solution as described in Eq. (30), which assures that the spacecraft do not drift away from each other. This completes the discussion of the differential energy corrections using orbital elements. These results demonstrate that equivalent answers can be obtained using the equations/solutions available in both frameworks, thereby providing additional insight on the periodicity constraint obtained using the linearized equations of relative motion.

Modeling Error Effects

Fuel optimal aperture forming is crucial for space applications because fuel is a very precious resource on-orbit. However, ignoring even a very small eccentricity in the reference orbit, for example, $e = 0.005$, typical of shuttle missions, can result in considerable relative motion errors in the passive apertures. These errors in general cause the spacecraft to drift away from the desired formation and, thus, would require corrective thruster firings. Also with an eccentric reference orbit, Eqs. (13–15) show that the shape of the closed-form solution is not a perfect ellipse, but is actually skewed and scaled. Thus, any formation-keeping algorithm that does not account for the changes due to eccentricity will have to work against the natural motion of the vehicles. Both of these errors will result in a continuous depletion of the fuel.

This section investigates the errors in the desired relative motion that result from assuming a circular reference orbit. Two distinct types of modeling errors are usually observed:

1) A formation initialization based on a circular orbit assumption typically results in differential energy errors. This error is observed as two different types of motion relative to the formation center, an in-track drift and a change in the size of the periodic relative motion.

2) As discussed, the shape of a closed-form solution based on an eccentric formation center is not a perfect ellipse. Also, the firings to form relative motion ellipses based on a circular orbit assumption⁷ would actually result in a different periodic relative motion pattern (in both the in-plane and cross-track directions). These both result in relative motion errors.

This section analyzes these modeling errors in three main parts. The first two parts show the effect of differential energy and relative motion errors on the relative motion in the in-plane and cross-track

directions. The third part presents numerical results based on a simple control algorithm using an underlying circular orbit assumption. Note that although all earlier analysis was presented for $0 < e < 1$, this section focuses on cases with $e \ll 1$ to simplify the expressions for the modeling errors.

Differential Energy Errors

To identify the modeling errors, the homogenous solutions in Eqs. (13) and (14) can be rewritten in terms of the periodic, that is, cos and sin, parts and terms that are a function of $H(\theta)$

$$x(\theta)_j = H(\theta) \left[2d_{2j}e^2 \sin(\theta) \right] + \sin \theta [d_{1j}e] - \cos \theta \left[\frac{d_{2j}e}{(1+e \cos \theta)^2} + d_{3j} \right] \quad (53)$$

$$y(\theta)_j = H(\theta) [2d_{2j}e(1+e \cos \theta)] + \sin \theta \left[\frac{d_{3j}}{(1+e \cos \theta)} + d_{3j} \right] + \cos \theta [d_{1j}e] + \left[d_{1j} + \frac{d_{4j}}{(1+e \cos \theta)} \right] \quad (54)$$

The only terms that can result in drift are the ones associated with $H(\theta)$, and, from Eq. (16), the corresponding drift term is $H_{\text{drift}}(\theta) = (1-e^2)^{-5/2} [3eE/2]$. $H_{\text{drift}}(\theta)$ grows linearly with the eccentric anomaly E and is also a monotonic function of θ [see Eq. (17)]. The analysis in the initialization section showed that a periodic motion requires that the terms associated with $H(\theta)$ be eliminated, which is accomplished by setting $d_{2j} = 0$. This constraint is equivalent to the differential energy matching conditions, as identified in the general initialization section. However, a modeling error in the reference orbit can result in a differential energy error (corresponding to $d_{2j} \neq 0$). As shown in Eq. (54), the result would be a drift in the in-track (y) direction. This drift would be accompanied by a secular periodic motion [periodic motion with increasing amplitude due to the influence of $H(\theta)$] in both the radial (x) and in-track (y) directions. However, as shown in Eqs. (53) and (54), this periodic motion would be scaled by an additional factor of $e \ll 1$.

An analytic solution can be developed for the expected drift rates if the nonzero reference orbit eccentricity is ignored. Consider a formation initialization maneuver at a desired radial separation $x(0)$ (chosen at $\theta = 0$ to simplify the analysis). An in-track impulsive firing is needed to zero the differential energy of the two spacecraft. With these initial conditions, Eq. (25) can be used to predict the expected drift per orbit as

$$\delta y(2\pi)_{\text{drift}} = w_{42} [p_{22}x(0) + p_{23}y'(0)] \quad (55)$$

For this initialization approach, $x(0)$ is the semiminor axis of the expected relative motion ellipse in the xy plane. If a circular orbit assumption had been made, that is, $e = 0$, then the in-track firing would be performed to set $y'(0) = -2x(0)$. However, if the reference orbit is actually eccentric, then, by the use of the expressions for w_{42} , p_{22} , and p_{23} , the drift would be

$$\delta y(2\pi)_{\text{drift}} = 2eH(2\pi)(1+e) \times \left[\frac{(2+e)(1+e)^2}{e^2} x(0) + \frac{(1+e)^3}{e^2} y'(0) \right] \quad (56)$$

$$= -\frac{6\pi e^2(1+e)}{(1-e^2)^{5/2}} \left[\frac{(2+e)(1+e)^2}{e^2} - \frac{2(1+e)^3}{e^2} \right] x(0) \quad (57)$$

$$= \frac{6\pi e(1+e)^3}{(1-e^2)^{5/2}} x(0) \quad (58)$$

If $0 < e \ll 1$ is assumed, the drift observed during aperture forming would be approximately

$$\delta y_{\text{drift per orbit}} \cong 6\pi e x_0 \quad (59)$$

which assumes that at $\theta = 0$ a circular orbit assumption was made and the natural frequency of the circular orbit was set equal to

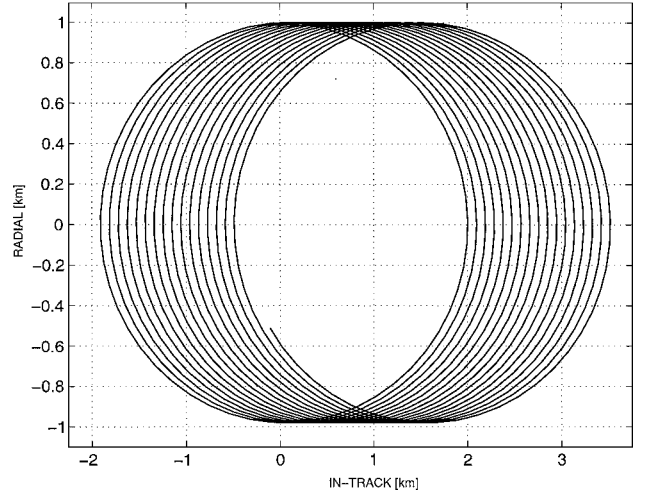


Fig. 10 In-plane modeling error effect $e = 0.005$.

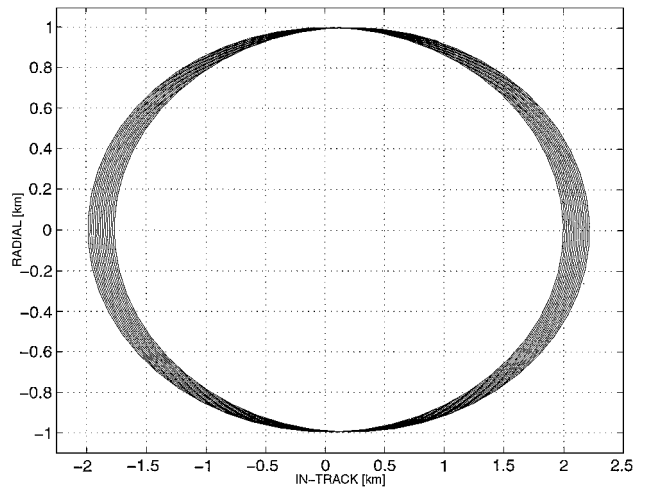


Fig. 11 In-plane differential J_2 effect $e = 0.005$.

the angular velocity of the actual eccentric orbit at $\theta = 0$, that is, $n_{\text{circ}} = \dot{\theta}(0)$.

To analyze the impact of this drift rate, consider a simple formation of two spacecraft initialized with 1-km radial and 0.6-km cross-track separation. The relative in-track velocity is set based on the assumption of a circular reference orbit. The reference orbit ($a = 6900$ km and $i = 52$ deg) actually has $e = 0.005$, which corresponds to a modeling error. The orbits of the two spacecraft were propagated in a high precision propagator and the relative motion results are shown in Fig. 10. These results clearly illustrate that, instead of a closed ellipse, the relative positions of the spacecraft drift in the in-track direction. In fact, after 16 orbits (≈ 1 day), the drift corresponds to roughly 75% of the original baseline, which is consistent with the predictions from Eq. (59) ($16 \times 6\pi e x_0 \approx 1.5$ km). This drift is removed if the initial relative velocity is modified as given in Eq. (30); the solution tracks the desired periodic relative orbital motion.

To further illustrate the significance of this modeling error, it can be compared to other large relative disturbances, such as the differential J_2 . Figure 11 shows the effect of differential J_2 on the formation during 16 orbits. For this case the formation was initialized using the corrected initialization (to account for $e \neq 0$), but the simulation included the effects of differential J_2 . When compared with Fig. 10, these results clearly show that ignoring the reference orbit eccentricity can dominate the differential disturbances.

A second type of initialization error could occur if the natural frequency n_{circ} of the circular reference orbit is set to be the natural frequency of the eccentric reference orbit n , that is, setting $n_{\text{circ}} \equiv n$. With the same type of analysis shown earlier, (see Appendix B for details), the drift in this case would be

$$\delta y(2\pi)_{\text{drift per orbit}_2} \cong -18\pi e x(0) \quad (60)$$

which is a factor of 3 larger than the preceding case.

The ΔV to perform the correct initialization [Eq. (30)] differs by only a factor of e from the firings designed using a circular reference orbit assumption because (see Appendix B)

$$\dot{y}_{\text{ecc}}(0) - \dot{y}_{\text{circ}}(0) \cong -3n x(0)e \quad \text{for } e \ll 1 \quad (61)$$

However, this (possibly larger) fuel burn ensures that the spacecraft attains the desired relative motion and will not drift from the formation center (in the absence of any additional disturbances). As is shown later in this section, this change in the fuel burn is significantly smaller than would be expected for a simple control scheme that constantly attempts to correct for these drift errors using a circular orbit assumption.

Relative Motion Errors: In-Track and Radial

The following investigates the in-plane relative motion errors using a slightly different formation initialization approach, but, as before, it is assumed that the reference orbit eccentricity is ignored in the design. In particular, consider the effect of setting the natural frequency of the circular reference orbit n_{circ} equal to the frequency n of the eccentric reference orbit, that is, $n_{\text{circ}} = n$, which is the same assumption used to derive the drift formula in Eq. (60).

To determine the initialization approach, consider the well-known homogenous solutions to the relative motion with a circular reference orbit¹⁷ (x is radial, and y is in-track)

$$x(t) = \frac{\dot{x}_0}{n_{\text{circ}}} \sin n_{\text{circ}} t - \left(\frac{2\dot{y}_0}{n_{\text{circ}}} + 3x_0 \right) \cos n_{\text{circ}} t + \left(\frac{2\dot{y}_0}{n_{\text{circ}}} + 4x_0 \right) \quad (62)$$

$$y(t) = \frac{2\dot{x}_0}{n_{\text{circ}}} \cos n_{\text{circ}} t + \left(\frac{4\dot{y}_0}{n_{\text{circ}}} + 6x_0 \right) \sin n_{\text{circ}} t + \left(y_0 - \frac{2\dot{x}_0}{n_{\text{circ}}} \right) - (3\dot{y}_0 + 6n_{\text{circ}} x_0) t \quad (63)$$

Given that the spacecraft is initially separated by $2b_0$ in the in-track direction from the formation center, ($y_0 = 2b_0$, $x_0 = 0$, $\dot{x}_0 = 0$, $\dot{y}_0 = 0$), assume that the goal of the initialization is to generate a relative periodic motion ellipse with semimajor axis $2b_0$ in the xy relative motion plane. However, once again, the initialization process will be based on the assumption of a circular reference orbit. (Note that $\theta = 0$ was selected to simplify the following analysis and to yield compact representations of the associated errors. The approach shown could be used to develop equivalent results for any θ .) In this case, to obtain a $2b_0 \times b_0$ relative motion ellipse centered at the origin of the formation center, a radial firing of $\dot{x}_0 = nb_0$ is initially applied to the spacecraft (recall the assumption that $n_{\text{circ}} = n$). As a result of the radial firing at $\theta = 0$ there is no violation of the periodicity constraint, that is, $d_{2j} = 0$, for the linearized equations of motion. However, in this case, the size of the relative motion ellipse would not be correct because, for an eccentric reference orbit, the angular velocity of the reference orbit $\dot{\theta}$ is not a constant. In fact, it can be shown that a firing of $\dot{x}(0) = \dot{\theta}(0)y(0)/2 = \dot{\theta}(0)b_0$ would actually result in a relative motion that is symmetric about the formation center at the origin, that is, $y(\pi) = -y(0) = -2b_0$. However, a radial firing of $\dot{x}_0 = nb_0$ results in a shape error since (see Appendix B)

$$y_{\text{err}}(\pi) = y(\pi) - y_{\text{des}} \cong 4ey(0) \quad (64)$$

Because $y_{\text{err}}(2\pi) = 0$, this corresponds to an error of $2ey(0)$ in the observed semimajor axis. For an eccentricity of $e = 0.005$ and semimajor axis of $y(0) = 2b_0 = 200$ m, this would result in a 2-m error (1% decrease of the semimajor axis). Also note that $y(\pi)$ will be shifted 4 m from its desired location at $-2b_0$. A similar analysis in Appendix B for the x direction shows that the semiminor axis error would be on the order of 1 m for this case.

As with the preceding example, the ΔV to initialize using the eccentric reference orbit analysis also differs by only a factor of e from the firings designed using a circular reference orbit assumption because (see Appendix B)

$$\dot{x}_{\text{ecc}}(0) - \dot{x}_{\text{circ}}(0) \cong ney(0) \quad \text{for } e \ll 1 \quad (65)$$

Notice that after the correct initialization, the relative motion would not be a perfect ellipse (it will follow its own natural motion), as indicated by the homogenous solutions given in Eqs. (13) and (14). However, it would be symmetric and have the desired semimajor and semiminor axis values.

Relative Motion Errors: Cross-Track

As noted earlier, the equations of motion in the cross-track direction [Eq. (12)] decouple from the in-plane motion as a result of the linearization. Thus, the error analysis can also be done separately for this direction. Because the motion in the cross-track direction is periodic with no drift terms [see Eq. (15)], the modeling errors discussed earlier would lead to relative motion errors. Note that the homogenous solution to the cross-track Hill's equation is¹⁹

$$z(t) = (\dot{z}_0/n_{\text{circ}}) \sin n_{\text{circ}} t + z_0 \cos n_{\text{circ}} t \quad (66)$$

If the initial condition is $z(0) = 0$, then with a circular reference orbit, the required cross-track firing to create periodic relative motion of amplitude c_0 at $\theta = \{\pi/2, 3\pi/2\}$ would be $\dot{z}_0 = c_0 n$ (assuming $n_{\text{circ}} = n$). However, this will be incorrect because the reference orbit is actually eccentric, the firing should actually be $\dot{z}_0 = c_0 \dot{\theta}(0)/(1+e)$ (see Appendix B). The error resulting from this incorrect firing is symmetric and can be approximated as

$$z_{\text{err}}(\pi/2) = z(\pi/2) - z_{\text{des}}(\pi/2) = -ec_0 = -z_{\text{err}}(3\pi/2) \quad (67)$$

For $e = 0.005$ and $c_0 = 200$ m, the cross-track relative motion error would be on the order of 1 m. Equations (64), (67), (B11), and (B13) provide a detailed analysis of the modeling errors associated with a circular orbit assumption. The following section analyzes the effect of these modeling errors on the fuel budget using a simple feedback control scheme.

Effect on Fuel Usage

In a feedback control system it is expected that the results of these initialization errors would be corrected at the expense of extra fuel. To demonstrate this idea, consider a simple formation-keeping algorithm based on a circular reference orbit assumption that is employed after the initialization. In this algorithm, formation keeping is done using a series of impulsive thruster firings at the location of initialization and its conjugate point on the reference orbit. The approach is to calculate the corrective impulse vector so that this correction takes the vehicle from the current location to the desired location in one-half of an orbit. To be consistent with the earlier analysis, assume that the thruster firings are calculated using the state propagation based on a circular reference orbit, that is, using Eqs. (62) and (63) instead of the eccentric ones, Eqs. (13) and (14).

First consider the periodic relative motion ellipse example given in the relative motion errors section. Because there are no differential energy errors in this case, the error associated with an incorrect radial firing is periodic. As a result, additional radial firings are required to correct the semimajor axis (nominally $2b_0$) of the relative motion ellipse at $\theta = i\pi$ and $\theta = (i+1)\pi$, for $i = \{1, 2, \dots\}$. For an arbitrary i , the radial firing $\delta\dot{x}(i\pi)$ is used at time $\theta = (i)\pi$ to correct for the error resulting from the firing at $\theta = (i-1)\pi$ and to make sure that the relative motion ellipse is the correct size at $\theta = (i+1)\pi$. Unfortunately, this firing introduces other errors because the correction is designed using the dynamics associated with a circular reference orbit. As a result, another correction will be required at $\theta = (i+1)\pi$, and this will introduce similar errors. Thus, the system would enter a cyclic error correction pattern (limit cycle) that results in continuous fuel depletion.

The fuel cost for formation keeping based on the initialization with only a radial firing was calculated numerically. A series of

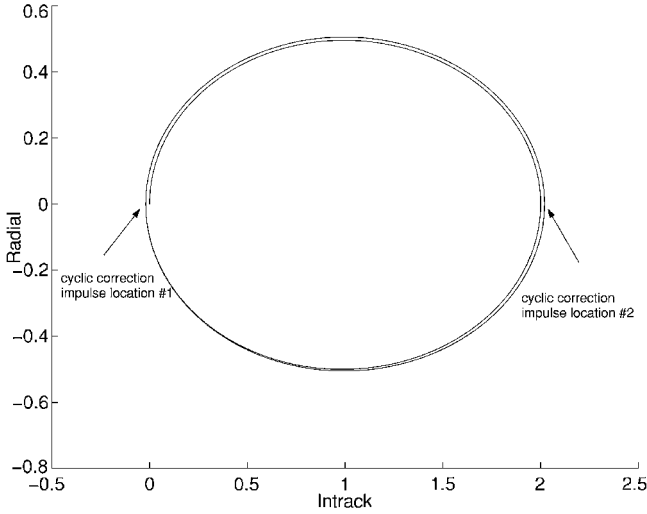


Fig. 12 Limit-cycle behavior for modeling error ($e = 0.01$), radial thruster firing.

simulations were performed for many cases with ranging values of e and b_0 . The resulting fuel burn was found to be approximately

$$\Delta V_{\min \text{ per orbit}} = \delta \dot{x}_{\text{per orbit}}^r \cong 3b_0 n e \quad (68)$$

to correct for the size of the relative motion ellipse. Equation (68) indicates that the fuel used is a linear function of e and the aperture size b_0 , which is the semiminor axis of the 2×1 relative motion ellipse. Figure 12 shows a typical limit cycle behavior observed using this simple control algorithm.

For the aperture forming case with in-track firing as discussed in the differential energy equalization section, there will be both differential energy and relative motion errors that result from the circular orbit assumption. Simulations were performed of the control algorithm described earlier (using in-track firings) for many values of e and b_0 . In this case, the necessary corrections were predicted to be

$$\delta \dot{y}_{\text{per orbit}}^i \cong 2\delta \dot{x}_{\text{per orbit}}^r, \quad \delta \dot{x}_{\text{per orbit}}^i \cong 2\pi \delta \dot{x}_{\text{per orbit}}^r \quad (69)$$

where $\delta \dot{y}_{\text{per orbit}}^i$ is used to correct the differential energy errors and $\delta \dot{x}_{\text{per orbit}}^i$ is used to correct for the drift effect on the relative motion ellipse. Firings are made at $\theta = (2i \pm \frac{1}{2})\pi$ per orbit. The simulations predicted a fuel usage for this case of

$$\Delta V_{\max \text{ per orbit}} \cong 8\Delta V_{\min \text{ per orbit}} \quad (70)$$

which is almost an order of magnitude higher as a result of the secular drift associated with the differential energy errors. For example, with an aperture semiminor axis of $b_0 = 1000$ m and the natural frequency associated with an 800-km circular orbit, an eccentricity error of $e = 0.001$ would result in $\Delta V_{\max \text{ per orbit}} \cong 2.6$ cm/s and $\Delta V_{\min \text{ per orbit}} \cong 0.35$ cm/s for this particular feedback control scheme.

These two final examples were designed to show the difficulties associated with using a simple feedback correction scheme that is based entirely on the circular reference orbit assumption to correct for these modeling errors. Obviously, different implementations of the error correction and firing patterns would change the fuel usage. However, the results of these examples do show that the reference orbit eccentricity could have an important effect on the fuel budget of a formation flying mission if not correctly accounted for in the control design.

Conclusions

This paper generalizes previous aperture design approaches and presents a complete initialization procedure for a fleet of vehicles with an eccentric reference orbit, for example, Molniya. The main result of the paper is derived in two ways. The primary analysis uses the solutions of the linearized equations of relative motion with respect to an eccentric reference orbit. These solutions are used to

find the necessary and sufficient conditions on the initial states that produce periodic solutions, that is, the vehicles return to the initial relative states at the end of each orbit. In the second method, the orbital elements are used to derive the exact nonlinear condition that ensures periodic relative motion from the differential energy matching condition. By the use of a consistent linearization approximation, it is then shown that an equivalent set of initialization conditions can be obtained in this second framework. This connection provides additional insight on the periodicity constraint obtained using the linearized equations of motion.

The paper also presents analytic formulas showing the type and magnitude of formation errors that can result from using a circular reference orbit assumption. These errors are verified in a nonlinear simulation and compared to other differential disturbances, for example, J_2 , for a typical low-Earth-orbit formation with in-plane and out-of-plane components. The drift results show that ignoring the reference orbit eccentricity (for $e \approx 10^{-3}$ and aperture size ≈ 1000 m) can be a dominant additional source of error. A simple control scheme was also used to evaluate the closed-loop response when there is a modeling error in the reference orbit, for example, the control design incorrectly assumes $e = 0$. Simulation results provide bounds on the fuel usage to account for the resulting modeling errors. The results clearly show that the modeling errors (and how they are handled) can have a large impact on the fuel usage for formation flying control.

Appendix A: Monodromy Matrix

The closed-form solutions for the in-plane and out-of-plane true anomaly rate of change of relative distances are given by

$$\begin{aligned} x'(\theta)_j &= \cos\theta [d_{1j}e + 2d_{2j}e^2 H(\theta)] + \sin\theta [2d_{2j}e^2 H'(\theta)] \\ &+ \sin\theta \left[\frac{d_{2j}e}{(1+e\cos\theta)^2} + d_{3j} \right] - \cos\theta \left[\frac{2d_{2j}e^2 \sin\theta}{(1+e\cos\theta)^3} \right] \end{aligned} \quad (A1)$$

$$\begin{aligned} y'(\theta)_j &= \left[\frac{d_{4j}e \sin\theta}{(1+e\cos\theta)^2} + 2d_{2j}e H'(\theta) \right] \\ &+ \cos\theta \left[\frac{d_{3j}}{(1+e\cos\theta)} + d_{3j} \right] + \sin\theta \left[\frac{d_{3j}e \sin\theta}{(1+e\cos\theta)^2} \right] \\ &- \sin\theta [d_{1j}e + 2d_{2j}e^2 H(\theta)] + \cos\theta [2d_{2j}e^2 H'(\theta)] \end{aligned} \quad (A2)$$

$$\begin{aligned} z'(\theta)_j &= \cos\theta \left[\frac{d_{5j}}{(1+e\cos\theta)} \right] + \sin\theta \left[\frac{d_{5j}e \sin\theta}{(1+e\cos\theta)^2} \right] \\ &- \sin\theta \left[\frac{d_{6j}}{(1+e\cos\theta)} \right] + \cos\theta \left[\frac{d_{6j}e \sin\theta}{(1+e\cos\theta)^2} \right] \end{aligned} \quad (A3)$$

$$H'(\theta) = \frac{\cos\theta}{(1+e\cos\theta)^3} \quad (A4)$$

$$H''(\theta) = \frac{-\sin\theta(1+e\cos\theta) + 3e\cos\theta \sin\theta}{(1+e\cos\theta)^4} \quad (A5)$$

The initial and final states can then be written as a function of the integration constants:

$$x'(0) = ed_{1j}, \quad x(0) = -\frac{e}{(1+e)^2}d_{2j} - d_{3j} \quad (A6)$$

$$y'(0) = \frac{2e}{(1+e)^2}d_{2j} + \frac{(2+e)}{(1+e)}d_{3j}$$

$$y(0) = (1+e)d_{1j} + \frac{1}{(1+e)}d_{4j} \quad (A7)$$

$$d_{1j} = \frac{1}{e}x'(0), \quad d_{2j} = \frac{(2+e)(1+e)^2}{e^2}x(0) + \frac{(1+e)^3}{e^2}y'(0) \quad (A8)$$

$$d_{3j} = -\frac{(1+e)}{e}y'(0) - \frac{2(1+e)}{e}x(0)$$

$$d_{4j} = (1+e)y(0) - \frac{(1+e)^2}{e}x'(0) \quad (\text{A9})$$

$$x'(2\pi) = ed_{1j} - \frac{6e^3\pi(1+e)}{(1-e^2)^{\frac{5}{2}}}d_{2j}$$

$$x(2\pi) = -\frac{e}{(1+e)^2}d_{2j} - d_{3j} \quad (\text{A10})$$

$$y'(2\pi) = \frac{2e}{(1+e)^2}d_{2j} + \frac{(2+e)}{(1+e)}d_{3j} \quad (\text{A11})$$

$$y(2\pi) = (1+e)d_{1j} + \frac{1}{(1+e)}d_{4j} - \frac{6e^2\pi(1+e)}{(1-e^2)^{\frac{5}{2}}}d_{2j} \quad (\text{A12})$$

With these expressions, the following presents the general form of the monodromy matrix. The simplified form is given in the paper as Eq. (24),

$$\begin{bmatrix} x'(2\pi) \\ x(2\pi) \\ y'(2\pi) \\ y(2\pi) \end{bmatrix}_j = \begin{bmatrix} w_{11}p_{11} & w_{12}p_{22} & w_{12}p_{23} & 0 \\ 0 & w_{22}p_{22} + w_{23}p_{32} & w_{22}p_{23} + w_{23}p_{33} & 0 \\ 0 & w_{32}p_{22} + w_{33}p_{32} & w_{32}p_{23} + w_{33}p_{33} & 0 \\ w_{41}p_{11} + p_{41}w_{44} & w_{42}p_{22} & w_{42}p_{23} & w_{44}p_{44} \end{bmatrix} \times \begin{bmatrix} x'(0) \\ x(0) \\ y'(0) \\ y(0) \end{bmatrix}_j \quad (\text{A13})$$

Evaluate each term in the matrix to get

$$w_{11}p_{11} = e \left[\frac{1}{e} \right] = 1$$

$$w_{12}p_{22} = \left[-\frac{6e^3\pi(1+e)}{(1-e^2)^{\frac{5}{2}}} \right] \left[\frac{(2+e)(1+e)^2}{e^2} \right]$$

$$= -\frac{6e\pi(1+e)^{\frac{1}{2}}(2+e)}{(1-e)^{\frac{5}{2}}}$$

$$w_{12}p_{23} = \left[-\frac{6e^3\pi(1+e)}{(1-e^2)^{\frac{5}{2}}} \right] \left[\frac{(1+e)^3}{e^2} \right] = -\frac{6e\pi(1+e)^{\frac{3}{2}}}{(1-e)^{\frac{5}{2}}}$$

$$w_{22}p_{22} + w_{23}p_{32} = \left[-\frac{e}{(1+e)^2} \right] \left[\frac{(2+e)(1+e)^2}{e^2} \right]$$

$$+ [-1] \left[\frac{-2(1+e)}{e} \right] = 1$$

$$w_{22}p_{23} + w_{23}p_{33} = \left[\frac{-e}{(1+e)^2} \right] \left[\frac{(1+e)^3}{e^2} \right]$$

$$+ [-1] \left[\frac{-(1+e)}{e} \right] = 0$$

$$w_{32}p_{22} + w_{33}p_{32} = \left[\frac{2e}{(1+e)^2} \right] \left[\frac{(2+e)(1+e)^2}{e^2} \right]$$

$$+ \left[\frac{(2+e)}{(1+e)} \right] \left[\frac{-2(1+e)}{e} \right] = 0$$

$$w_{32}p_{23} + w_{33}p_{33} = \left[\frac{2e}{(1+e)^2} \right] \left[\frac{(1+e)^3}{e^2} \right] + \left[\frac{(2+e)}{(1+e)} \right]$$

$$\times \left[\frac{-(1+e)}{e} \right] = 1$$

$$w_{41}p_{11} + p_{41}w_{44} = [(1+e)] \left[\frac{1}{e} \right] + \left[\frac{1}{(1+e)} \right]$$

$$\times \left[\frac{-(1+e)^2}{e} \right] = 0$$

$$w_{42}p_{22} = \left[-\frac{6e^2\pi(1+e)}{(1-e^2)^{\frac{5}{2}}} \right] \left[\frac{(2+e)(1+e)^2}{e^2} \right]$$

$$= -\frac{6\pi(2+e)(1+e)^{\frac{1}{2}}}{(1-e)^{\frac{5}{2}}}$$

$$w_{42}p_{23} = \left[-\frac{6e^2\pi(1+e)}{(1-e^2)^{\frac{5}{2}}} \right] \left[\frac{(1+e)^3}{e^2} \right] = -\frac{6\pi(1+e)^{\frac{3}{2}}}{(1-e)^{\frac{5}{2}}}$$

$$w_{44}p_{44} = \left[\frac{1}{(1+e)} \right] [(1+e)] = 1$$

Appendix B: Modeling Errors

Derivation of Equation (60)

For the second type of initialization error discussed in the last part of the paper, it is assumed that $n_{\text{circ}} = n$. Then, because $\dot{y}(t) = y'(\theta)\dot{\theta}$, the correction of $\dot{y}(0) = -2nx(0)$ actually results in $y'(0) = -2x(0)n/\theta(0)$. Let $\alpha = n/\theta(0)$, then this quantity can be estimated as

$$\alpha = \frac{n}{\theta(0)} = \frac{(1-e^2)^{\frac{3}{2}}}{(1+e)^2} = \frac{(1-e)^{\frac{3}{2}}}{(1+e)^{\frac{1}{2}}} \cong 1 - 2e \quad \text{for } e \ll 1 \quad (\text{B1})$$

When Eq. (B1) is used and $y'(0)$ is replaced with the new initialization $y'(0) = -2\alpha x(0)$ in Eq. (56), the drift is

$$\delta y(2\pi)_{\text{drift}} \cong -\frac{6\pi e^2(1+e)}{(1-e^2)^{\frac{5}{2}}}$$

$$\times \left[\frac{(2+e)(1+e)^2}{e^2} - \frac{2(1+e)^3(1-2e)}{e^2} \right] x(0)$$

$$= -\frac{6\pi(1+e)^3}{(1-e^2)^{\frac{5}{2}}} [(2+e) - 2(1+e)(1-2e)] x(0)$$

$$\cong -\frac{6\pi(1+e)^3}{(1-e^2)^{\frac{5}{2}}} 3ex(0) \cong -18\pi ex(0) \quad (\text{B2})$$

Derivation of Equation (61)

Analyzing the difference of Eq. (30) and the circular orbit assumption initialization $\dot{y}_{\text{circ}}(0) = -2nx(0)$ gives the error in the initialization firing

$$\dot{y}_{\text{ecc}}(0) - \dot{y}_{\text{circ}}(0) = -nx(0) \left[\frac{(2+e)}{(1+e)^{\frac{1}{2}}(1-e)^{\frac{3}{2}}} - 2 \right]$$

$$= -nx(0) \left[\frac{(2+e) - 2(1+e)^{\frac{1}{2}}(1-e)^{\frac{3}{2}}}{(1+e)^{\frac{1}{2}}(1-e)^{\frac{3}{2}}} \right]$$

$$\cong -3nx(0)e \quad \text{for } e \ll 1 \quad (\text{B3})$$

Derivation of Equation (64)

To find $y(\pi)$ resulting from the incorrect firing at $\theta=0$, first calculate the integration constants of the homogenous solutions. Because $d_{2j}=0$ (as a result of no differential energy errors) and $y'(0)=0$ (initial condition), the homogenous solutions for $y'(\theta)$ in

Appendix A can be used to show that $d_{3j} = 0$. The homogenous solutions for $x'(\theta)$ and $y(\theta)$ with $\theta = 0$ give

$$x'(\theta) = ed_{1j}, \quad y(\theta) = (1+e)d_{1j} + d_{4j}/(1+e) \quad (B4)$$

which can be rewritten as

$$d_{1j} = x'(\theta)/e, \quad d_{4j} = y(\theta)(1+e) - (1+e)^2[x'(\theta)/e] \quad (B5)$$

Finally, evaluating the homogenous solutions at $\theta = \pi$ yields

$$x'(\pi) = -ed_{1j}, \quad y(\pi) = (1-e)d_{1j} + d_{4j}/(1-e) \quad (B6)$$

Rewriting $y(\pi)$ as a function of the initial conditions gives

$$y(\pi) = -x'(\theta)[4/(1-e)] + y(0)[(1+e)/(1-e)] \quad (B7)$$

If the incorrect initialization was used (i.e., setting $\dot{x}(0) = ny(0)/2$ instead of using the correct initialization, which is $\dot{x}(0) = \dot{\theta}(0)y(0)/2$), then Eq. (B7) takes the following form

$$y(\pi) = -y(0)\frac{2n}{\dot{\theta}(0)(1-e)} + y(0)\frac{(1+e)}{(1-e)} = y(0)\frac{(1+e) - 2\alpha}{(1-e)} \quad (B8)$$

where $\dot{x}(t) = x'(\theta)\dot{\theta}(\theta)$; $\alpha = n/\dot{\theta}(0) \cong 1 - 2e$ was defined earlier. The error associated with the incorrect initialization can then be computed as

$$\begin{aligned} y_{\text{err}}(\pi) &= y(\pi) - y_{\text{des}} = y(0)\frac{(1+e) - 2\alpha}{(1-e)} - [-y(0)] \\ &= -y(0)\frac{1-5e}{1-e} + y(0) \\ &\cong -y(0)(1-4e) + y(0) = 4ey(0) \end{aligned} \quad (B9)$$

The same procedure can be repeated to check for the error in the semiminor axis x at $\theta = \pi/2$ and $3\pi/2$

$$x(\pi/2) = d_{1j}e = \alpha[y(0)/2] \cong (1-2e)[y(0)/2] \quad (B10)$$

$$x_{\text{err}}(\pi/2) = x(\pi/2) - x_{\text{des}}(\pi/2) \cong -ey(0) \quad (B11)$$

$$x(3\pi/2) = -d_{1j}e = -\alpha[y(0)/2] \cong -(1-2e)[y(0)/2] \quad (B12)$$

$$x_{\text{err}}(3\pi/2) = x(3\pi/2) - x_{\text{des}}(3\pi/2) \cong ey(0) \quad (B13)$$

where $x_{\text{des}}(\pi/2) = y(0)/2$ and $x_{\text{des}}(3\pi/2) = -y(0)/2$.

Derivation of Equation (65)

An analysis of the fuel can be done in the x direction. In this case, the difference between the correct firing and the firing designed using the circular reference orbit assumption is

$$\dot{x}_{\text{ecc}}(0) - \dot{x}_{\text{circ}}(0) = \frac{y(0)}{2}[\dot{\theta}(0) - n] = \frac{y(0)n}{2}\left[\frac{(1+e)^2}{(1-e)^{\frac{3}{2}}} - 1\right] \quad (B14)$$

$$= \frac{y(0)n}{2}\left[\frac{(1+e)^{\frac{1}{2}} - (1-e)^{\frac{3}{2}}}{(1-e)^{\frac{3}{2}}}\right] \quad (B15)$$

$$\cong \frac{y(0)n}{2}2e = y(0)ne \quad \text{for } e \ll 1 \quad (B16)$$

Derivation of Equation (67)

Calculating the integration constant d_{5j} at $\theta = 0$ from Eq. (A3) and using $\dot{z} = z'\dot{\theta}$ yields

$$d_{5j} = \frac{\dot{z}(0)(1+e)}{\dot{\theta}(0)} \quad (B17)$$

By the use of the incorrect firing $\dot{z}(0) = c_0n$ in d_{5j} , the homogenous solution for z in Eq. (15) at $\theta = \pi/2$ and $3\pi/2$ can be calculated as

$$z(\pi/2) = c_0(1+e)[n/\dot{\theta}(0)] \cong c_0(1+e)(1-2e) \cong c_0(1-e) \quad (B18)$$

$$z(3\pi/2) = -c_0(1+e)[n/\dot{\theta}(0)] \cong -c_0(1+e)(1-2e) \cong -c_0(1-e) \quad (B19)$$

and the error in the relative periodic motion is

$$z_{\text{err}}(\pi/2) = z(\pi/2) - z_{\text{des}}(\pi/2) \cong -ec_0 \quad (B20)$$

$$z_{\text{err}}(3\pi/2) = z(3\pi/2) - z_{\text{des}}(3\pi/2) \cong ec_0 \quad (B21)$$

where $z_{\text{des}}(\pi/2) = c_0 = -z_{\text{des}}(3\pi/2)$. If the correct firing of $\dot{z}(0) = c_0\theta(0)/(1+e)$ had been used, then the resulting motion would be periodic motion with amplitude c_0 .

Acknowledgments

Funded in part under U.S. Air Force Grant F49620-99-1-0095 [Marc Jacobs (U.S. Air Force Office of Scientific Research) and Rich Burns (U.S. Air Force Research Laboratory)] and NASA Goddard Space Flight Center (GSFC) Grant NAG5-6233-0005 [John Bristow, Jesse Leitner, and Frank Bauer (NASA GSFC)]. The authors would like to thank the anonymous reviewers for their very helpful comments.

References

- ¹Bauer, F. H., Bristow, J., Folta, D., Hartman, K., Quinn, D., and How, J. P., "Satellite Formation Flying Using an Innovative Autonomous Control System (AUTOCON) Environment," AIAA Paper 97-3821, Aug. 1997.
- ²Bauer, F. H., Hartman, K., and Lightsey, E. G., "Spaceborne GPS: Current Status and Future Visions," *ION-GPS Conference*, Inst. of Navigation, Alexandria, VA, 1998, pp. 1493-1508.
- ³Bauer, F. H., Hartman, K., How, J. P., Bristow, J., Weidow, D., and Busse, F., "Enabling Spacecraft Formation Flying Through Spaceborne GPS and Enhanced Automation Technologies," *ION-GPS Conference*, Inst. of Navigation, Alexandria, VA, 1999, pp. 369-384.
- ⁴Das, A., and Cobb, R., "TechSat21—Space Missions Using Collaborating Constellations of Satellites," *12th Annual Small Satellite Conference*, Paper SSC98-VI-1, AIAA, Reston, VA, Aug. 1998.
- ⁵Robertson, A., Inalhan, G., and How, J. P., "Spacecraft Formation Flying Control Design for the Orion Mission," *Proceedings of the AIAA Guidance, Navigation, and Control Conference*, AIAA, Reston, VA, 1999, pp. 1562-1575.
- ⁶Inalhan, G., Busse, F. D., and How, J. P., "Precise Formation Flying Control of Multiple Spacecraft Using Carrier-Phase Differential GPS," *Proceedings of the AAS/AIAA Spaceflight Mechanics Meeting*, AIAA, Reston, VA, 2000, pp. 151-165.
- ⁷Sedwick, R., Miller, D., and Kong, E., "Mitigation of Differential Perturbations in Synthetic Apertures Comprised of Formation Flying Satellites," *Advances in Astronautical Sciences: Space Flight Mechanics 1999*, Vol. 102, Pt. 1, Univelt, San Diego, CA, 1999, pp. 323-342.
- ⁸Schaub, H., and Alfriend, K., " J_2 Invariant Relative Orbits for Spacecraft Formations," *Flight Mechanics Symposium*, Paper 11, NASA Goddard Space Flight Center, Greenbelt, MD, May 1999.
- ⁹Lawden, D. F., *Optimal Trajectories for Space Navigation*, Butterworths, London, 1963, pp. 79-86.
- ¹⁰Carter, T. E., and Humi, M., "Fuel-Optimal Rendezvous near a Point in General Keplerian Orbit," *Journal of Guidance, Control, and Dynamics*, Vol. 10, No. 6, 1987, pp. 567-573.
- ¹¹Carter, T. E., "New Form for the Optimal Rendezvous Equations near a Keplerian Orbit," *Journal of Guidance, Control, and Dynamics*, Vol. 13, No. 1, 1990, pp. 183-186.
- ¹²Sabol, C., Burns, R., and McLaughlin, C., "Satellite Formation Flying Design and Evolution," *Journal of Spacecraft and Rockets*, Vol. 38, No. 2, 2001, pp. 270-278.
- ¹³Roger, A., and McInnes, C., "Safety Constrained Free-Flyer Path Planning at the International Space Station," *Journal of Guidance, Control, and Dynamics*, Vol. 23, No. 6, 2000, pp. 971-979.
- ¹⁴Melton, R., "Time-Explicit Representation of Relative Motion Between Elliptical Orbits," *Journal of Guidance, Control, and Dynamics*, Vol. 23, No. 4, 2000, pp. 604-610.
- ¹⁵Marec, J. P., *Optimal Space Trajectories*, Elsevier, New York, 1979, pp. 130-154.
- ¹⁶Bate, R. R., Mueller, D. D., and White, J. E., *Fundamentals of Astrodynamics*, Dover, New York, 1971, pp. 20, 25-33, 212-222, 396-412.
- ¹⁷Chobotov, V. A., *Orbital Mechanics*, 2nd ed., AIAA Educational Series, AIAA, Reston, VA, 1996, pp. 155-158, 162-164, 168-181.
- ¹⁸Rugh, W. J., *Linear System Theory*, 2nd ed., Prentice-Hall, Upper Saddle River, NJ, 1996, pp. 81-87.
- ¹⁹Hale, J. K., and Koçak, H., *Dynamics and Bifurcation*, Springer-Verlag, New York, 1991, Chap. 11.